Inertial oscillations of a pinned dislocation

M. Bhattacharya,[1,*] A. Dutta,[2] P. Mukherjee,[1] N. Gayathri,[1] and P. Barat[1]
[1]*Variable Energy Cyclotron Centre, 1/AF, Bidhannagar, Kolkata 700064, India*
[2]*Department of Metallurgical and Materials Engineering, Jadavpur University, Kolkata 700032, India*
(Received 29 July 2010; revised manuscript received 28 September 2010; published 19 November 2010)

A pinned dislocation segment is well known to oscillate under external cyclic load in the phenomenon of internal friction of solids. In this paper, we observe in the molecular-dynamics simulations, the occurrence of damped oscillations of pinned dislocations even under the applied constant load. For a given link length l, the fundamental oscillation frequency f_0 is found to deviate significantly from the f_0 vs l relation predicted from the traditional Koehler's vibrating string model. This is attributed to the coupling among the oscillating dislocation segments, which is realized by modifying the boundary conditions in the Koehler's equation of motion.

DOI: 10.1103/PhysRevB.82.184113 PACS number(s): 61.72.Lk, 02.70.Ns, 61.72.Qq

I. INTRODUCTION

Plastic deformation of a crystalline solid is typically mediated by the motion of line defects called dislocations.[1] However, these line defects do not move seamlessly throughout the crystal and often encounter many obstacles during their motion. These obstacles, which can be point defects, voids, precipitates, and even other dislocations, can pin down the motion of a moving dislocation.[2–5] In particular, the event of pinning becomes frequent during strain hardening resulting from the reduction in the mean-free path of the mobile dislocations[6,7] and its kinetic energy is liberated as the dislocation comes to rest. In case of plastic deformation, it is generally believed that a moving dislocation spends most of its time at the pinning site until the local resolved shear stress exceeds the critical depinning stress for that particular pinning obstacle. As in the general theory of kinetics, the slowest step is regarded as the rate controlling step, the thermodynamic model of dislocation mediated plasticity[8] considers the pinning-depinning process to be a key factor governing the rate of plastic deformation. Besides, dislocation pinning is a compulsory ingredient of the phenomenon of internal friction of solids.[1,9] In the studies of internal friction, the strong obstacles clamp the ends of a dislocation segment, whereas the weaker ones exert extra drag force on the vibrating dislocation.[10] Much of the research work in this direction has primarily focused on the process of depinning and its relation with the nature of the obstacles,[3,11–13] while the dynamics of dislocation pinning at the ultra-fine scales of length and time has not attracted much attention of the dislocation physicists. Maintaining a skeptical outlook on this lack of interest, we study the phenomenon of dislocation pinning, down to the atomistic level through the molecular-dynamics (MD) simulations. Moreover, the Koehler's vibrating string model is used as a mathematical tool to analyze and understand the simulation outcome. As presented below, the combined approach of MD simulation and mathematical analysis reveal significant nontrivial features of dislocation dynamics, which hitherto remained obscured.

II. SIMULATION PROCEDURE AND RESULTS

To explore the dynamics of dislocation pinning and eventually perceive the MD results within the framework of Koehler's model, it is preferable to choose a simple dislocation structure. Therefore, we consider an edge dislocation in bcc system and perform our case studies in two different systems, molybdenum (Mo) and tungsten (W), where both the crystals are constructed employing the widely used Finnis-Sinclair potential model[14] with the corresponding parameters. The MD simulations in this work are performed using the MD++ molecular-dynamics package.[15] The cell dimensions for Mo are shown in Fig. 1(a), where the Burgers vec-

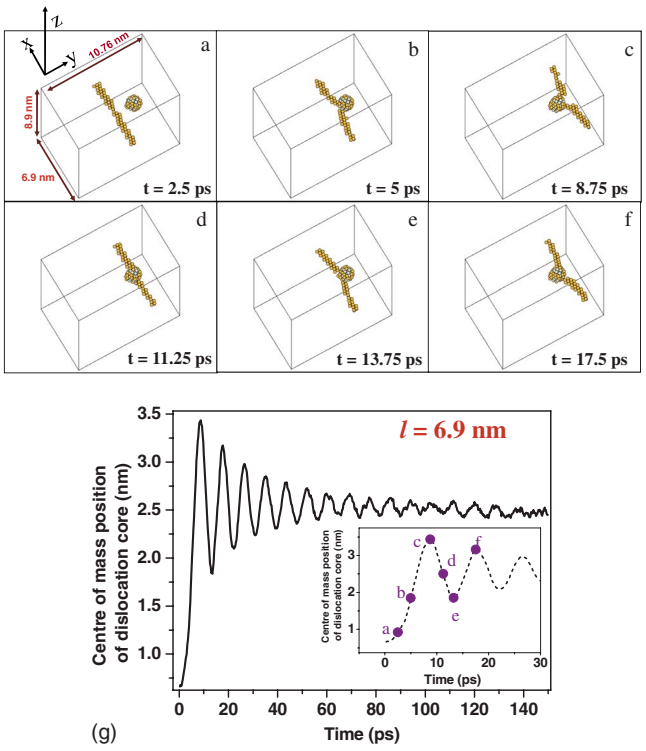

FIG. 1. (Color online) Storyboard of dislocation pinning in molybdenum. [(a)–(f)] Snapshots of dislocation void interaction and subsequent oscillations at different time steps at 100 K. (g) The oscillatory motion of the pinned segment is visible through the position of the center of mass of the dislocation core atoms with respect to time. The positions corresponding to the MD snapshots are indicated in the inset.

tor $b=a\langle 111\rangle/2$ ($a=0.314\ 72$ nm is the lattice constant) of the dislocation is along the y direction and its line is along the x direction. The y and z dimensions are $39.5a\langle 111\rangle/2$ and $20a\langle \bar{1}01\rangle$, respectively, where the x dimension along $\langle 1\bar{2}1\rangle$ is varied to alter the link length (l). A nanovoid of diameter ~ 1 nm, which acts as a reasonably strong pinning obstacle, is introduced 2.5 nm away from the dislocation line and the periodic boundary condition is imposed except along the z direction. The whole system is equilibrated at a constant temperature by means of the Nosé-Hoover thermostat[16] and then the atoms at free boundaries are subjected to precisely calculated forces, so that a shear stress of 50 MPa is created and maintained throughout the simulation.[17] The atomic coordinates are calculated with the time step of 0.5 fs using the velocity verlet integrator.[17] The dislocation core atoms are identified by using the suitable filtering window of width 0.024–0.1 nm^2 of centrosymmetric deviation parameter[17] and the dislocation position is defined as the center of mass of the core atoms, which is recorded at 0.25 ps time interval. We have repeated these simulations at different temperatures within a range from 50 to 300 K. Similarly, MD simulations are carried out for W with a lattice constant of $a=0.316\ 52$ nm.

Figures 1(a)–1(f) show the snapshots of a typical simulation run at 100 K for Mo. Under the effect of the shear load τ and drag coefficient B, the dislocation with effective mass M per unit length, attains a terminal velocity $v_0=\tau b/B$, before its motion is suddenly hindered by the pinning obstacle. It is interesting to observe that instead of loosing all of its kinetic energy instantly, the pinned dislocation segment exhibits oscillatory dynamics.[18] The y coordinate of the center of mass of the atoms of the dislocation core is displayed as a function of elapsed time in Fig. 1(g), where one can easily recognize that the dislocation segment comes to rest by means of damped oscillations. Oscillations of pinned dislocations are common in the studies of internal friction and ultrasonic attenuation.[19,20] However, they are essentially forced oscillations of dislocations induced by the external cyclic loads. Surprisingly, what we discover here are the spontaneous oscillations of a pinned dislocation segment under the applied constant load. The frequency of oscillation can be calculated from the fast Fourier transform (FFT) of the MD simulation data as demonstrated in Fig. 2(a). We obtain the fundamental frequencies (f_0) for different link lengths l of the dislocation varying from 3.9–23.1 nm and represent the observation as the f_0^2 vs l^{-2} plot in Fig. 2(b). Similar feature has also been observed for W. The reason for this particular choice of representation will be apparent in the following part of the paper, where we further investigate the dynamics through analytical modeling.

III. ANALYTICAL MODEL

We begin with the typical string model of vibrating dislocations first introduced by Koehler[21] and further developed by Granato and Lücke[22] to analyze the internal friction of solids. According to this model, the dynamics of a dislocation segment can be described as

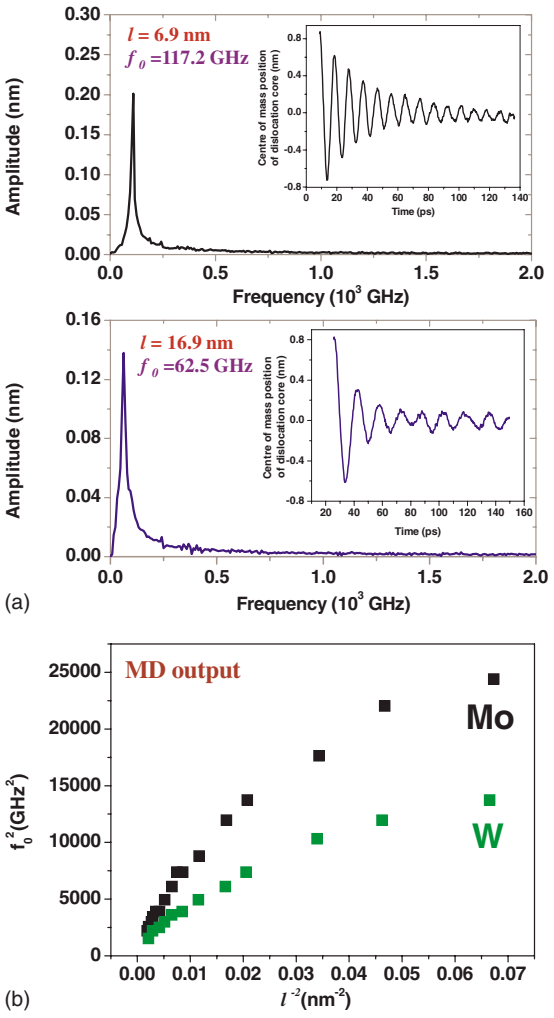

FIG. 2. (Color online) (a) Typical frequency spectra of oscillation data for Mo for two different link lengths with 2^9 data points used for each FFT analysis. The inset shows the raw data after removing the initial part up to the first oscillation peak and bringing the data to the zero mean value. The longer link length produces low frequency oscillation. (b) f_0^2 as obtained from the frequency spectra are plotted against l^{-2} for Mo and W.

$$M\frac{\partial^2 y}{\partial t^2}+B\frac{\partial y}{\partial t}-T\frac{\partial^2 y}{\partial x^2}=\tau b, \tag{1}$$

where $y(x,t)$ is the displacement of dislocation along the y direction at time t and T is the line tension. In the framework of the MD simulation scheme, we assume that the moving dislocation line is incident on the obstacles with velocity v_0. With l as the link length, the boundary conditions compatible with the MD simulation schemes are

$$y(0,t)=0, \quad y(l,t)=0 \tag{2}$$

and the initial conditions are

$$y(x,0)=0, \quad \frac{dy(x,0)}{dt}=v_0[u(x)-u(x-l)], \tag{3}$$

where $u(x)$ stands for the unit step function. Under these conditions, the auxiliary equation produces the following so-

lution for the center of mass position of the oscillating string (see Appendix A):

$$y_{cm}(t) = \sum_{m=0}^{\infty} \frac{8v_0 l}{(2m+1)^2\pi^2\sqrt{(2m+1)^2\pi^2c^2 - \eta^2 l^2}} \times e^{-\eta t} \sin\left(\sqrt{\frac{(2m+1)^2\pi^2c^2}{l^2} - \eta^2}\right)t, \quad (4)$$

where $c=\sqrt{T/M}$ and $\eta=B/2M$. Correspondingly, the first harmonic is the most prominent frequency component and is given by $y_{cm}(t)=\frac{8v_0 l}{\pi^2\sqrt{\pi^2c^2-\eta^2 l^2}}e^{-\eta t}\sin(\sqrt{\frac{\pi^2c^2}{l^2}-\eta^2})t$. Equation (4) clearly shows that the dislocation segment executes damped inertial oscillations driven by the initial momentum of the moving dislocation even under non cyclic load and hence the oscillations are inertial. The term $e^{-\eta t}$ reflects the dissipative work done by the frictional forces of the medium on the string; in other words, the kinetic energy of the dislocation gets dissipated in the form of heat. We find that a larger ratio of the drag coefficient to the effective mass causes faster damping with smaller oscillation amplitude and the rate of damping increases significantly with rise in temperature.[18] The oscillation profile in Fig. 1(g) shows a perfect exponential damping and can be used to estimate the effective linear density of the dislocation, which in our case[18] turns out to be 3.7×10^{-16} kg/m for Mo. Similar exponential fitting to the oscillation data for W is used[18] to obtain the effective linear density of the dislocation as 10.5×10^{-16} kg/m. The order of effective masses are comparable to that reported for other materials.[23]

Having established the damped inertial oscillations of dislocation after pinning, it is crucial to investigate the fitness of the employed mathematical formalism in dealing with the actual underlying dynamics. For nonzero shear stress, the particular integral in the solution of Eq. (1) merely decides the phase of the oscillations without affecting the frequency. The fundamental frequency f_0 obtained from Eq. (4) predicts the f_0^2 vs l^{-2} plot to be linear, which is certainly not observed in Fig. 2(b). Curious about this anomaly in the frequency plot, we explore if there is a room for modification in the existing formalism.

The f_0^2 vs l^{-2} relation is the manifestation of the fact that the end points of the vibrating string are ideally clamped. Thus, the boundaries are completely reflective with no transmittance, thereby creating standing waves with natural frequency $f_0=\pi c/l$. A deviation from this behavior is the signature of partial transmittance of the boundaries, which signifies some extent of flexibility of the clamped ends. In presence of such flexible clamping, the oscillation of a clamped string segment remains no more independent; rather, it gets coupled with the vibrations from the other segments. In order to depict this concept analytically, we propose to realize this coupling by modeling the ends of the vibrating string segment as clamped to Hookean springs with stiffness constant k (refer to Fig. 3). We consider an array of springs clamped with the string at positions periodically separated by the gap l. For identical initial conditions for each of the string segment, the dynamics of each segment would also be identical. In this context, the Koehler's equation of motion must be solved with the boundary conditions

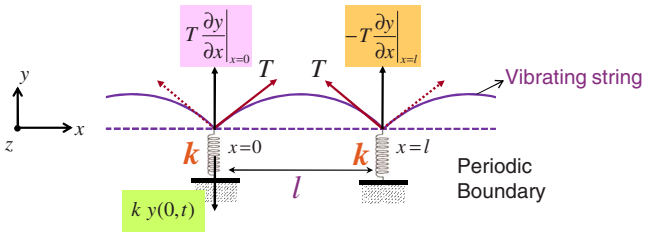

FIG. 3. (Color online) Schematic of the flexible boundary condition modeled as the ends of the vibrating segments attached with springs.

$$y(0,t) = y(l,t),$$

$$T\left(\frac{\partial y}{\partial x}\right)_{x=0} - T\left(\frac{\partial y}{\partial x}\right)_{x=l} = ky(0,t), \quad (5)$$

along with the initial conditions

$$y(x,0) = 0, \quad \frac{dy(x,0)}{dt} = v_0. \quad (6)$$

The flexible boundary conditions lead to a significantly different relation between f_0 and l in terms of the wave vector p as (see Appendix B)

$$\Gamma(l,p,T) = 2pT\tan(pl/2) = k, \quad (7)$$

which is nonlinear and an exact solution cannot be derived. In particular, for large extent of coupling, i.e., for small value of the spring constant, Eq. (7) can be approximated as $2pT\tan(pl/2)\simeq p^2Tl=k$ which gives the smallest and dominant frequency component $f_0=\sqrt{p^2c^2-\eta^2}/2\pi = \sqrt{(kM^{-1}l^{-1}-\eta^2)}/2\pi$. We find that the modifications in the boundary conditions are extremely significant as they are capable of altering the $f_0^2\propto l^{-2}$ relation to a drastically different $f_0^2\propto l^{-1}$.

IV. NUMERICAL IMPLEMENTATION OF MODIFIED BOUNDARY CONDITIONS

In order to confirm the mathematical inferences, we numerically solve Eq. (1) with flexible periodic boundaries. This is implemented by discretizing the string as an array of closely spaced beads of some specific mass, representing the linear density of the string. Each bead is connected to the neighboring beads through massless string under a given tension and the trajectories of the beads are calculated using the Velocity-Verlet integrator.[17] Here we assume the beads of unit mass to be separated by unit distance (arbitrary unit). In case of perfect boundaries, the end point coordinates remain invariant, whereas for flexible boundaries, Hookean restoring forces are added. The viscous drag coefficient and the line tension are 0.2 and 1000, respectively (both in arbitrary units), for the results presented in Figs. 4(a)–4(c). This approximation is justified as it can be proved[24] that the resulting dynamics converges to that of a string of homogeneous

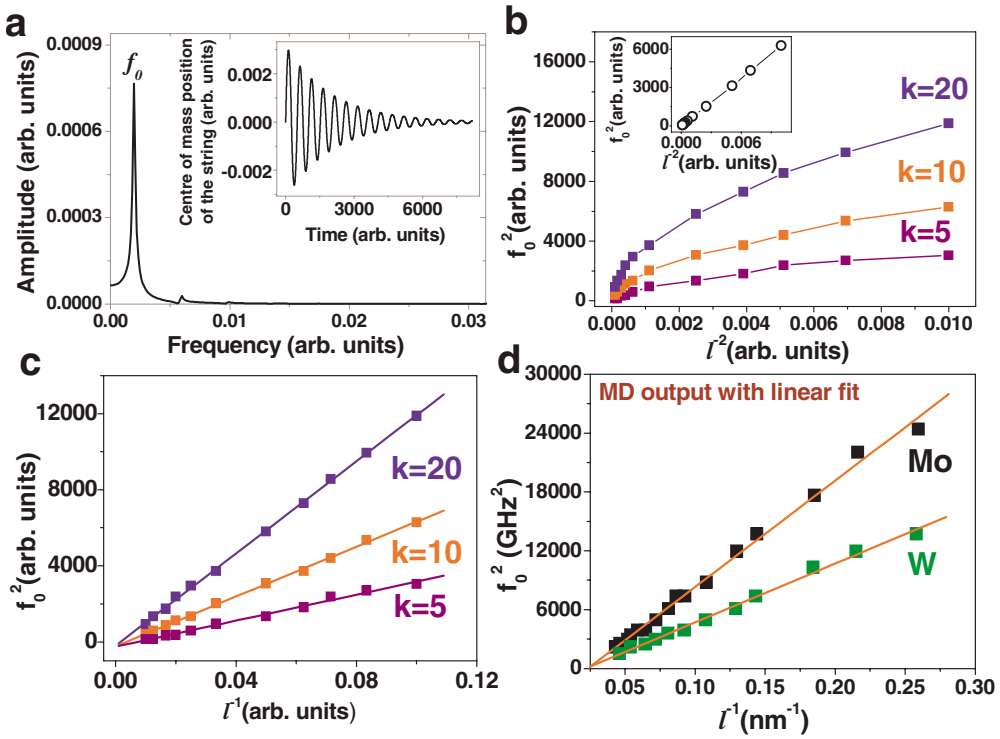

FIG. 4. (Color online) Numerical implementation of the flexible boundary model with $M=1$, $B=0.2$, and $T=1000$, all in arbitrary units. (a) Damped oscillations (inset) and the frequency spectrum with 2^{13} data points for the spring constant $k=10$. (b) f_0^2 vs l^{-2} plot with three different values of k. The result for the rigid boundary condition is given in the inset. A resemblance in the trends between Figs. 2(b) and 4(b) is noticeable. (c) f_0^2 vs l^{-1} plot has been presented with the linear fits. (d) f_0^2 vs l^{-1} plots of the MD data [already presented in Fig. 2(b)] with linear fits to extract the effective spring constants from the slopes for Mo and W.

mass density in the limit where the number of beads tends to infinity. This numerical solution successfully reproduces the damped oscillations as shown in Fig. 4(a). We produce the f_0^2 vs l^{-2} plot in Fig. 4(b) for the spring constants $k=5$, 10, and 20 to facilitate a direct comparison with Fig. 2(b). Moreover, as a strong coupling is predicted to result in a linear relation between f_0^2 and l^{-1}, we rescale the abscissa of Fig. 4(b) from l^{-2} to l^{-1} [refer Fig. 4(c)] and observe that the linearity is indeed prominent. Surprisingly, this linearity is found even in the MD results as presented in Fig. 4(d). This provides a firm ground for expecting a sufficiently large coupling of oscillators, quantifiable in terms of the spring constant. The linear fits to the MD output estimate the effective spring constants to be 1.54 and 2.48 N/m for Mo and W, respectively. This physically signifies springs of very small stiffness constants and hence justifies a large coupling among the oscillating dislocation segments. One can now figure out that the trend in Fig. 4(d), as obtained from the atomistic simulations reveals that the dynamics should be more appropriately described in the architecture of flexible boundary model, instead of the conventional one.

V. DISCUSSION

An important issue is yet to be resolved. We know that Koehler's equation is justifiable for a pinned dislocation because of its direct correspondence with a clamped string under tension. The linear density of the string is analogous to the effective mass of the dislocation, the coefficient of viscosity corresponds to dislocation drag[25] and the string's tension to the elastic energy per unit length increment of the dislocation line. As the MD simulation as well as the analytical approach highlight the suitability of the flexible boundary conditions, physical interpretation of the *spring* introduced in the model becomes essential. Each oscillating pinned dislocation segment acts as an emitter as well as a receiver of elastic waves. Such an oscillator interacts with the elastic waves emitted by the other oscillators (the image oscillators in these simulations) present in the system.[26] Owing to the finite velocity of these waves, the oscillator may be out of phase with a wave incident on it. Because of this phase mismatch, the stress waves effectively exert additional load on the oscillating pinned segment and it manifests in a work done against this load. This is analogous to the work done against the restoring forces of the springs depicted in the vibrating string model with flexible boundaries (Fig. 3). Thus the coupling of oscillations invoked through the springs is understandable as the coupling realized through the emitted elastic waves.

Interestingly, the inertial oscillations of dislocations were initially studied by Granato[27] through purely analytical methods in the context of plasticity of superconductors. In his paper, he arrived at the oscillatory solution using the rigid boundary conditions and obtained a linear relation between f_0 and l^{-1} [Eq. (6) in Ref. 27]. It was deduced that the ratio of dynamic to static pinning force is a function of the natural frequency of vibrating dislocations [Eqs. (9) and (10) in his

paper]. Moreover, the radiation damping was also found to depend on the this frequency [Eq. (12) in the paper]. As we show that the coupling among the vibrating dislocation segments may change the natural frequency, the aforementioned issues also need to be perceived in light of this concept. Besides the inertial oscillations, this conclusion is also significant for the forced oscillations in internal friction. The analysis assumes periodic boundaries to make it compatible with the MD scheme; nevertheless, the concept of interacting oscillations are equally valid for a distribution of link lengths and orientations.

VI. CONCLUSIONS

The present work reveals the occurrence of inertial oscillations of pinned dislocations in crystalline solids. The molecular-dynamics simulations are found to exhibit such oscillations for edge dislocation in molybdenum, an elastically anisotropic solid, as well as in tungsten, which is almost isotropic. Surprisingly, when this phenomenon is analyzed in terms of Koehler's vibrating string model,[21] the frequency-link length dependency obtained from MD data is found to deviate from the conventional $f_0^2 \propto l^{-2}$ relation for both the solids. We resolve this inconsistency by incorporating the effect of coupling between oscillating dislocation segments. This is analytically done by modifying the rigid boundary condition to the flexible boundary condition and $f_0^2 \propto l^{-1}$ relation has been derived. A noticeable feature of this modification is to quantify the extent of coupling in terms of the effective spring constants introduced in our model. The MD simulations, theoretical analysis, and the numerical implementation are in excellent agreement to validate our concepts. A more involved study on this aspect may need to treat the coupling in terms of the elastic field theory and include the statistical distributions of link lengths and the effective spring constants in this regard. In the same spirit, the effect of coupling in case of forced oscillations of dislocations merits further dedicated work.

ACKNOWLEDGMENTS

A.D. acknowledges the financial support from CSIR, India to carry out this research work.

APPENDIX A: VIBRATING STRING WITH RIGID BOUNDARIES

The Koehler's equation of motion is $M\frac{\partial^2 y}{\partial t^2}+B\frac{\partial y}{\partial t}-T\frac{\partial^2 y}{\partial x^2}=0$,which can be written as

$$\frac{\partial^2 y}{\partial t^2}+2\eta\frac{\partial y}{\partial t}-c^2\frac{\partial^2 y}{\partial x^2}=0, \tag{A1}$$

where $\eta=\frac{B}{2M}$ and $c=\sqrt{\frac{T}{M}}$. Using the variable separable method, we obtain the trial oscillatory solution

$$y(x,t)=e^{-\eta t}(C_1\cos px+C_2\sin px)\times(C_3\cos\omega t+C_4\sin\omega t), \tag{A2}$$

where p is the wave vector and $\omega^2=p^2c^2-\eta^2$. Rigid boundary conditions are

$$y(0,t)=0,\quad y(l,t)=0. \tag{A3}$$

Using condition 1 of Eq. (A3), we obtain $y(x,t)=C_2e^{-\eta t}\sin px(C_3\cos\omega t+C_4\sin\omega t)$, while condition 2 of Eq. (A3), gives $pl=n\pi$, where $n=1,2,3,\ldots$.

Finally we have

$$y(x,t)=\sum_{n=1}^{\infty}C_{2n}e^{-\eta t}\sin\frac{n\pi x}{l}\left(C_{3n}\cos\sqrt{\frac{n^2\pi^2c^2}{l^2}-\eta^2}t+C_{4n}\cos\sqrt{\frac{n^2\pi^2c^2}{l^2}-\eta^2}t\right). \tag{A4}$$

Arbitrary initial conditions are

$$y(x,0)=f(x),\quad \left(\frac{\partial y}{\partial t}\right)_{t=0}=g(x). \tag{A5}$$

From Eqs. (A4) and (A5) (condition 1) we get

$$f(x)=\sum_{n=1}^{\infty}A_n\sin\frac{n\pi x}{l},\quad A_n=C_{2n}C_{3n}.$$

We compare this with the half-range sine series to obtain

$$A_n=\frac{2}{l}\int_0^l f(x)\sin\frac{n\pi x}{l}dx. \tag{A6}$$

Using Eqs. (A4) and (A5) (condition 2), and Eq. (A6), we obtain

$$g(x)=\sum_{n=1}^{\infty}\left[C_{2n}C_{4n}\sqrt{\frac{n^2\pi^2c^2}{l^2}-\eta^2}-\eta A_n\right]\sin\frac{n\pi x}{l}.$$

Again from the half-range sine series

$$C_{2n}C_{4n}\sqrt{\frac{n^2\pi^2c^2}{l^2}-\eta^2}-\eta A_n=\frac{2}{l}\int_0^l f(x)\sin\frac{n\pi x}{l}dx.$$

Assuming $C_{2n}C_{4n}=B_n$, we can write

$$B_n=\frac{2}{\sqrt{n^2\pi^2c^2-\eta^2l^2}}\times\int_0^l[\eta f(x)+g(x)]\sin\frac{n\pi x}{l}dx. \tag{A7}$$

Collecting Eqs. (A4), (A6), and (A7), we have

$$y(x,t)=e^{-\eta t}\sum_{n=1}^{\infty}\sin\frac{n\pi x}{l}\left(A_n\cos\sqrt{\frac{n^2\pi^2c^2}{l^2}-\eta^2}t+B_n\cos\sqrt{\frac{n^2\pi^2c^2}{l^2}-\eta^2}t\right). \tag{A8}$$

After having formulated the generalized solution, we now consider our case study. The initial conditions compatible with the MD simulations are

$$f(x)=0,\quad g(x)=v_0[u(x)-u(x-l)].$$

Equations (A7) and (A8) yield

$$A_n = 0, B_n = \frac{4v_0 l}{(2m+1)\pi\sqrt{(2m+1)^2\pi^2c^2 - \eta^2 l^2}}, \quad \text{(A9)}$$

where $m = \frac{n-1}{2} = 0, 1, 2, \ldots$

From Eqs. (A8) and (A9) we find

$$y(x,t) = \sum_{m=0}^{\infty} \frac{4v_0 l}{(2m+1)\pi\sqrt{(2m+1)^2\pi^2c^2 - \eta^2 l^2}} e^{-\eta t} \times \sin\frac{(2m+1)\pi x}{l} \sin\left(\sqrt{\frac{(2m+1)^2\pi^2c^2}{l^2} - \eta^2}\right) t. \quad \text{(A10)}$$

The center of mass is evaluated as

$$y_{cm}(t) = \frac{1}{l}\int_0^l y(x,t)dx = \sum_{m=0}^{\infty} \frac{8v_0 l}{(2m+1)^2\pi^2\sqrt{(2m+1)^2\pi^2c^2 - \eta^2 l^2}} \times e^{-\eta t} \sin\sqrt{\frac{(2m+1)^2\pi^2c^2}{l^2} - \eta^2} t. \quad \text{(A11)}$$

The most prominent is the first harmonic with $m=0$. $y_{cm}(t) = \frac{8v_0 l}{\pi^2\sqrt{\pi^2c^2 - \eta^2 l^2}} e^{-\eta t} \sin \omega t$, where $\omega^2 = \omega_0^2 - \eta^2$ with natural frequency $\omega_0 = \pi c/l$.

APPENDIX B: VIBRATING STRING WITH FLEXIBLE PERIODIC BOUNDARIES

We begin with the trial solution

$$y(x,t) = e^{-\eta t}(C_1 \cos px + C_2 \sin px) \times (C_3 \cos \omega t + C_4 \sin \omega t). \quad \text{(B1)}$$

The boundary conditions are

$$y(0,t) = y(l,t) \quad \text{(B2)}$$

and

$$T\left[\left(\frac{\partial y}{\partial x}\right)_{x=0} - \left(\frac{\partial y}{\partial x}\right)_{x=l}\right] = ky(0,t), \quad \text{(B3)}$$

where k is the spring constant. Here Eq. (B2) indicates the periodic boundary condition. From Eqs. (B1) and (B2) we find

$$\frac{C_1}{C_2} = \frac{1 - \cos pl}{\sin pl}, \quad pl \neq n\pi, \quad n = 1,2,3\ldots. \quad \text{(B4)}$$

$pl = n\pi$ does not yield a meaningful result with Eqs. (B2) and (B3) and we proceed with Eq. (B4).

Using Eqs. (B1) and (B3) we have

$$\left[\frac{C_1}{C_2}(1 - \cos pl) + \sin pl\right] = k. \quad \text{(B5)}$$

Substituting Eq. (B4) into Eq. (B5) yields

$$2pT \tan\frac{pl}{2} = k. \quad \text{(B6)}$$

*mishreyee@veccal.ernet.in

[1] J. P. Hirth and J. Lothe, *Theory of Dislocations* (Wiley and Sons, New York, 1982).

[2] N. B. Meisner, D. S. Woo, H. B. Huntington, G. L. Salinger, R. W. Shaw, and L. V. Meisel, J. Phys. Chem. Solids **34**, 1399 (1973).

[3] T. Hatano and H. Matsui, Phys. Rev. B **72**, 094105 (2005).

[4] D. J. Bacon and Yu. N. Osetsky, J. Nucl. Mater. **329-333**, 1233 (2004).

[5] M. C. Fivel, C. R. Phys. **9**, 427 (2008).

[6] R. Vetter, R. H. J. Fastenau, and A. Van Den Beukel, Phys. Status Solidi **70**, 177 (1982).

[7] B. Devincre, T. Hoc, and L. Kubin, Science **320**, 1745 (2008).

[8] J. S. Langer, E. Bouchbinder, and T. Lookman, Acta Mater. **58**, 3718 (2010).

[9] A. V. Granato and K. Lücke, *Physical Acoustics* (Academic Press, New York, 1966), Vol. 4, Pt. A.

[10] T. Ö. Oğurtani, Phys. Rev. B **21**, 4373 (1980).

[11] R. O. Scattergood and D. J. Bacon, Acta Metall. **30**, 1665 (1982).

[12] S. Zapperi and M. Zaiser, Mater. Sci. Eng., A **309-310**, 348 (2001).

[13] B. Bakó, M. Zaiser, D. Weygand, M. Samaras, and W. Hoffelner, J. Nucl. Mater. **385**, 284 (2009).

[14] M. W. Finnis and J. E. Sinclair, Philos. Mag. A **50**, 45 (1984).

[15] http://micro.stanford.edu

[16] S. Nosé, Mol. Phys. **52**, 255 (1984); W. G. Hoover, Phys. Rev. A **31**, 1695 (1985).

[17] V. V. Bulatov and W. Cai, *Computer Simulations of Dislocations* (Oxford University Press, Oxford, 2006).

[18] See supplementary material at http://link.aps.org/supplemental/10.1103/PhysRevB.82.184113 for the movie clip, evaluation of effective masses and the other relevant simulation data.

[19] L. B. Magalas and S. Gorczyca, *Internal Friction and Ultrasonic Attenuation in Solids* (Trans Tech, Stafa-Zurich, 1993).

[20] M. S. Blanter, I. S. Golovin, H. Neuhäuser, and H.-R. Sinning, *Internal Friction in Metallic Materials: A Handbook* (Springer-Verlag, Berlin, 2007).

[21] J. S. Koehler, *Imperfections in Nearly Perfect Crystals* (Wiley and Sons, New York, 1952).

[22] A. V. Granato and K. Lücke, J. Appl. Phys. **27**, 583 (1956); **27**, 789 (1956).

[23] Erik Bitzek and Peter Gumbsch, Mater. Sci. Eng., A **400**, 40 (2005); Y. Cheng, E. Bitzek, D. Weygand, and P. Gumbsch, Modell. Simul. Mater. Sci. Eng. **18**, 025006 (2010).

[24] P. M. Morse and H. Feshbach, *Methods in Theoretical Physics: Part I* (McGraw-Hill, New York, 1953).

[25] V. I. Alshits and V. L. Indenbom, in *Dislocations in Solids*, edited by F. R. N. Nabarro (North-Holland, New York, 1986), Chap. 34.

[26] In the given MD scheme, an oscillator would also interact with the elastic waves reflected from the surfaces.

[27] A. V. Granato, Phys. Rev. B **4**, 2196 (1971).